CFD Letters

Journal homepage:
https://semarakilmu.com.my/journals/index.php/CFD_Letters/index
ISSN: 2180-1363

Effect of the Aligned Magnetic Field over a Stretching Sheet through Porous Media in Casson Fluid Flow

Ramanjana Koka[1,*], Aruna Ganjikunta[2]

[1] Department of Mathematics, School of Science, GITAM (Deemed to be University), Hyderabad, Telangana, India
[2] Department of Mathematics, St. Francis College for Women, Begumpet, Hyderabad – 500016, Telangana, India

ARTICLE INFO

Article history:
Received 22 June 2023
Received in revised form 19 July 2023
Accepted 20 August 2023
Available online 1 January 2024

Keywords:
Aligned Magnetic Field; Porous Medium; Casson Fluid; Dufour and Soret Effects; Prandtl Number

ABSTRACT

Researchers in the thermo-fluidic field have dedicated considerable effort to exploring methods for improving heat transfer in diverse thermal systems. Among these methods, incorporating porous mediums into thermal systems stands out as particularly effective. The movement of substances through these porous materials, which encompass both fluid and solid components, can be described by either assuming that both phases are at the same temperature or that they are at different temperatures. The significance of heat and mass flux arises from their association with chemical potential and temperature gradient respectively. These connections hold value within a wide array of fields, including electrical power generation, solar power technology, chemical engineering, petrology and many more. In the present study, aligned magnetic effects have been investigated on local thermal non-equilibrium (LTNE) circumstances on steady, incompressible, laminar flow of a non-Newtonian Casson fluid across a stretching sheet in a porous medium. The LTNE conditions are implemented to generate two distinct temperature profiles for both fluid and solid phases. By choosing appropriate similarity transformations, the governing partial differential equations are transformed into ordinary differential equations for the flow parameters and are solved using numerical method Runge-Kutta-4 with shooting technique. The flow attributes are thoroughly inspected graphically in response to the influence of the developing factors. As aligned magnetic parameter and porosity parameter values increase, heat transmission improves, but velocity decreases. In the flow zone, as values of angle increases, magnetic field intensity increased. The heat flux in both fluid and solid phases decreases as the Dufour number rises. As the Soret number rises, the mass transfer rate falls.

1. Introduction

Aligned magnetic field plays an important role in many areas of science and technology. These effects can influence the orientation and behaviour of magnetic particles, materials, or fluids. These aligned magnetic field effects on fluids have a range of important applications and are used to control and manipulate fluid motion and behaviour in a variety of contexts. It has significant implications for

* *Corresponding author.*
E-mail address: rkoka@gitam.in (Ramanjana Koka)

https://doi.org/10.37934/cfdl.16.4.1638

fluid dynamics to develop new technologies for energy generation, propulsion, and plasma control. When radiation, chemical reactions, and heat generation are all present together, Reddy *et al.,* [1] conducted a thorough investigation into the effects of an aligned magnetic field on the unsteady flow of a Casson fluid. Kumar *et al.,* [2] explained the reasons for an aligned magnetic field, Hall current, and thermal radiation on the magnetohydrodynamic MHD flow of Casson fluid along an inclined plate. R. Saravana *et al.,* [3] investigated the effect of cross-diffusion and magnetic field alignment on the Casson fluid flow over a stretched surface with a range of thicknesses. Reddy *et al.,* [4] examined the theoretical magnetohydrodynamic (MHD) effect of cross-diffusion and an aligned magnetic field effect along a stretched surface of varying thickness. Kodi *et al.,* [5] looked at the effect of a Soret-aligned magnetic field, chemical reaction, and unsteady hydrodynamic flow across an inclined plate submerged by porous media.

A porous medium is a material or substance that contains interconnected void spaces or pores through which fluids, such as gases or liquids, can flow. Porous media are commonly found in various natural and engineered systems, including soils, rocks, ceramics, foams, and filters. The physical properties of porous media, such as pore size, shape, and connectivity, play a crucial role in determining their overall behaviours, including flow of fluid, heat and mass fluxes. Heat transfer within a porous material can be done in two ways, as explained by Neild & Bejan [6]. In their work, they provided a local thermal equilibrium (LTE) model to solve the energy equation between a liquid and solid structure in a porous medium which is the first model. This LTE model is valid when there is a slight difference in temperature in a permeable zone between both solid and liquid phases. The second model that describes convective heat transmission in porous media is Local Thermal Non-Equilibrium (LTNE) model, which employs separate energy equations for both solid and liquid phases explained by Alhadhrami *et al.,* [7] where he investigated how the LTNE model is utilised to study fluid flow in porous media using the two temperature equations for both the liquid and solid phases. Sukumar Pati *et al.,* [8] also categorically discussed LTNE modelling strategies. Muthtamilselvan *et al.,* [9] and Prakash *et al.,* [10], both investigated a vertical stretching plate embedded in a scarcely packed porous medium used to study the effects of Brownian motion, thermophoresis, transitory local thermal non-equilibrium (LTNE), on laminar boundary layer flow of an incompressible, viscous nanofluid. Vaddemani *et al.,* [11] studied the effects of Soret on the unsteady free convection flow of a viscous incompressible fluid through a porous media with high porosity confined by a vertical infinite moving plate while being affected by thermal diffusion, chemical reaction, and heat source. Sama *et al.,* [12] studied a 2D steady flow model of carbon nanotubes-based nanofluids and heat transfer past a porous stretchable or shrinkable sheet.

Due to its significant and wide-ranging uses, research on nanofluids is becoming increasingly popular among scientists, particularly in the industrial and engineering fields. Investigating the effects of viscous loss caused by a sodium carboxymethyl cellulose (CMC-water) nanofluid holding copper nanoparticles at room temperature under convective boundary conditions (CBC) was explained by Mahat *et al.,* [13] and in his work a mathematical model for viscoelastic nanofluid flow moving closer to a linear horizontal circular cylinder in magnetohydrodynamics (MHD) was also developed again by Mahat *et al.,* [14]. Bakar *et al.,* [15] explored the flow and heat transfer in a micropolar fluid at the MHD stagnation point over an exponentially vertically stretching/shrinking sheet are explored. In an unsteady laminar magnetohydrodynamics (MHD) convective rotating flow, Aruna *et al.,* [16] investigated the influence of Hall and ion slip on the properties of a second-grade fluid while taking chemical reaction and radiation absorption into consideration. Raizah *et al.,* [17] explored the impact of an angled electromagnetic force on mixed convective processes in two-sided lid-driven geometries by employing local thermal nonequilibrium (LTNE) conditions and assumed a flow domain filled with a porous material in which the working fluids consist of magnetic micropolar

nanofluids comprising CuO nanoparticles and water as a base fluid are considered. Motsa *et al.,* [18] investigated the behaviour of impulsively begun vertical porous surfaces in non-Darcian MHD fluid flow. They have given consideration to the impact of thermophoresis, which results from colloidal particles migrating in response to a macroscopic temperature gradient. Sarada *et al.,* [19] investigated the properties of flow, heat, and mass transfer behaviour of non-Newtonian Jeffrey and Oldroyd-B fluids over a stretching sheet of permeable material using the Buongiorno model with the LTNE effect.

The Local Thermal Non-Equilibrium (LTNE) model has been extensively used by Parhizi *et al.,* [20] to predict convective heat transfer in porous media and author was certain about many of the earlier LTNE-based models relied on a constant Biot (Bi) number to capture thermal interactions between fluid and solid phases. For fully developed flow in a porous-medium-filled channel, where Bi varies along the channel, he suggested an LTNE model to account for this. They used the Boussinesq approximation and the Darcy rule to approximate the flow. Employing the finite difference method (FDM) and the LTNE model, Alsabery *et al.,* [21] described how to simulate the impact of uneven heating and a limited wall thickness on natural convection in a square porous chamber. The simulation involves heating a thin, horizontally oriented wall of the cavity, which has a limited thickness and can be heated either uniformly or non-uniformly. Meanwhile, vertical walls of the cavity are sustained at a constant, cold temperature.

By incorporating a thermal boundary condition model close to an impermeable wall, Ouyang *et al.,* [22] created Local Thermal Non-Equilibrium (LTNE) constraints for convective heat transformation in a porous medium. This model permits numerical simulations that can be employed for validation of the model by comparing it to pore-scale and macro-scale LTNE models. Furthermore, the spreading of heat flux between both solid and fluid phases is affected by the wall's tangential interfacial thermal resistance, which is thought to exist in this instance.

Researchers' interest in non-Newtonian fluid fluxes has lately increased due to the expanding number of economic and technical uses for these flows. The non-Newtonian fluid flows near stretched sheets have implications for environmental and geophysical processes, such as in the transport of pollutants in rivers, oil spills on water surfaces, and lava flows on volcanic slopes. Consequently, studies on the rate of heat transfer, fluid flow dynamics, and a wide range of practical applications require a fundamental knowledge of the flow field of non-Newtonian fluids at the boundary layer close to the stretched surface.

Pramanik *et al.,* [23] investigated Casson fluid as a class of non-Newtonian fluid. In Casson fluid, the yield stress manifests itself in a certain way. Casson fluid is a shear-thinning liquid with infinite viscosity at zero rates of shear, and zero viscosity at infinite rates of shear, below which no flow occurs. Liquids like blood, honey, concentrated juice, and other similar substances are known as Casson liquids. Casson introduced this viscoelastic liquid model in 1995, particularly describing sticky slurries. Mohamed *et al.,* [24] examined effects of slip on boundary layer flow and heat transmission on a horizontal flat surface submerged in Casson ferrofluid based on blood. Numerical analysis is done on the magnetite and cobalt ferrite ferroparticles suspended in the Casson fluid, which is analogous to human blood K A Khan *et al.,* [25], in their study found that the model has been enhanced to predict high shear-rate viscosities even when there is a dearth of additional shear-rate data. Mukhopadhyay *et al.,* [26] studied the Casson liquid flow on various surfaces taking into account different influencing factors. Hamid *et al.,* [27] looked at how linear thermal radiation affected both steady and erratic flow when a uniform magnetic field was present. They created a dual solution for the heat transfer rate and Casson fluid flow in 2D magnetohydrodynamics (MHD) across a stretched sheet. The Magnetohydrodynamic (MHD) of Casson fluid flow through a porous linear stretching sheet that occurs in two lateral directions was inspected by Nadeem *et al.,* [28].

Mustafa *et al.,* [29] gave information on the direction of a stretching sheet caused by a Casson fluid moving close to a downtrend point by examining heat transfer properties with viscous dissipation. In a double stratified form, mixed convection MHD Casson fluid flow towards an inclined stretched cylindrical surface is explored by Rehman *et al.,* [30], and the manifestations of the flow field scenario that result from heat generation/absorption and chemical interactions are noted.

Dufour effect is a heat flow resulting from a chemical potential gradient. Diffusion flows referred as thermal diffusion, Soret effect, or diffusion thermos are produced by a gradient in the thermal profile or temperature profile. Hayat *et al.,* [31] analysed the influence of the Soret and Dufour for magnetohydrodynamic (MHD) flow of the Casson fluid across a stretched surface. Ramzan *et al.,* [32] examined magnetohydrodynamic (MHD) mixed convection Casson fluid flow across an inclined flat plate. While studying this current flow issue, the heat source/sink, impacts of thermal radiation, chemical reaction, and heat transfer are all considered. The combined effects of Soret, Dufour, and chemical processes, Kumar *et al.,* [33] studied characteristics of the heat and mass transfer rate in Casson fluid flow driven by MHD natural convection via permeable vertical plate.

The convective heat and mass transfer rates for external interface layer can alter in response to changes in the surface mass flow, often known as blowing. Evaporation can occasionally cause a significant transfer of species. The blowing effect is brought on by Stefan, an issue for species transmission. Puneeth *et al.,* [34] explored a 3D bio-convective flow of a Casson nanofluid carrying gyrotactic microorganisms over a vertically stretched sheet creating an induced magnetic field. These microorganisms work as bioactive mixers by circulating owing to bioconvection, which stabilises nanoparticle suspension in the solution. Dual factors of thermophoresis and Random Walk, as well as Stefan blowing, are all taken into consideration in their mathematical model. Uddin *et al.,* [35] investigated Stefan blowing effect, second-order velocity slip, temperature slip, and microbial species slip on a nonlinear bioconvection boundary layer flow over a horizontal plate submerged in a porous medium which was done in passive controlled boundary conditions. Tuz Zohra *et al.,* [36] studied a viscous nanofluid's boundary layer flow under a magnetic field's influence. They used multiple slip conditions and Stefan-blowing effects to illustrate a mathematical model of constantly forced convection past a rotating disc submerged in a water-based nanofluid containing microorganisms. Latiff *et al.,* [37] described a theoretically and numerically mathematical model for the unstable forced convection over a spinning stretchable disc in a nanofluid, including microorganisms and accounting for the Stefan-blowing effect.

The study likely seeks to provide a comprehensive understanding of the combined effects of aligned magnetic fields, Casson fluid properties, and porous media on fluid flow behaviour, contributing to both fundamental fluid dynamics knowledge and potential practical applications.

The study aims to comprehensively explore the overall effects of an aligned magnetic field, stretching sheet, LTNE conditions, Stefan blowing, Soret, and Dufour effects on Casson liquid flow. It seeks to contribute to both theoretical knowledge and potential practical applications in fluid dynamics, engineering, and materials science.

The significance of incorporating an aligned magnetic field, LTNE conditions, Soret and Dufour effects into probing of Casson fluid flow lies in the ability to uncover new phenomena, enhance accuracy in modelling real-world situations, and provide valuable insights for various applications.

Research on the Casson liquid flow in an aligned magnetic field under stretched sheet circumstances with LTNE is uncommon. In this work, LTNE restrictions were used to analyse how an aligned magnetic field, rates of heat and mass transfer influenced Casson fluid flow along a stretched sheet of uniform thickness while being impacted by the Stefan Blowing, Soret, and Dufour effects. The impacts of flow field on essential parameters are examined.

2. Methodology

2.1 Mathematical Formulation

A Non-Newtonian Casson fluid flowing in a two-dimensional steady, incompressible laminar flow across a stretched sheet is considered. Cartesian coordinates convey the physical model in Figure 1. The stretching sheet velocity is measured as $U_w = cx$ (c is constant for stretching) which is parallel to the plane $y = 0$ and restricted to $y > 0$. The aligned magnetic field B_0 is applied, as illustrated in Figure 1, and it is expected that this aligned magnetic field will also exert an influence on the sheet. A homogeneous porous medium is considered. Additionally, when Soret and Dufour's effects occur, mass and heat movement mechanisms are considered. To calculate rate of heat transfer of both solid and fluid phases is assessed through two different temperature equations which are taken from a previous study [6,10]). Let V_w be the surface blowing velocity due to mass transfer and is proportional to the mass flux at the sheet's surface.

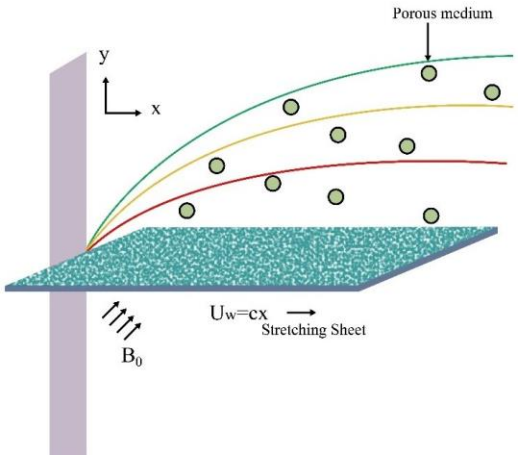

Fig.1. Flow Geometry [7]

Considering the following rheological equation of state for an isotropic, incompressible flow of a Casson fluid:

$$\tau_{ij} = \begin{cases} 2\left(\mu_B + \dfrac{P_y}{\sqrt{2\pi}}\right) e_{ij}, \pi > \pi_c \\ 2\left(\mu_B + \dfrac{P_y}{\sqrt{2\pi_c}}\right) e_{ij}, \pi_c > \pi \end{cases}$$

where $\pi = e_{ij}$, e_{ij} is the $(i,j)^{th}$ component of the deformation rate with itself, μ_B is the plastic dynamic viscosity of the non-Newtonian fluid, P_y is the fluid's yield stress, and π_c signifies a critical value of this product followed by non-Newtonian model taken from previous study of Yusof *et al.,* [38].

Governing equations for flow assumptions are made with an aligned angle $0 < \emptyset < \frac{\pi}{2}$, and rate of heat transfer operation in porous medium, based on Alhadhrami *et al.,* [7] with moderation:

$$\frac{\partial u}{\partial x} + \frac{\partial v}{\partial y} = 0 \tag{1}$$

$$\frac{1}{\varepsilon^2}\left[u\frac{\partial u}{\partial x} + v\frac{\partial u}{\partial y}\right] = \frac{u_f}{\rho_f}\left(1 + \frac{1}{\beta}\right)\left(\frac{\partial^2 u}{\partial y^2} + \frac{\partial^2 u}{\partial x^2}\right) - \frac{u_f}{\rho_f}\frac{u}{K'} - \frac{\sigma_f {B_0}^2 Sin^2\emptyset}{\rho_f}u, \tag{2}$$

$$\frac{1}{\varepsilon}\left[u\frac{\partial T_f}{\partial x}+v\frac{\partial T_f}{\partial y}\right]=\frac{k_f}{(\rho C_p)_f}\left(\frac{\partial^2 T_f}{\partial y^2}+\frac{\partial^2 T_f}{\partial x^2}\right)+\left(\frac{D_m k_T}{C_s C_p}\frac{\partial^2 C}{\partial y^2}\right)+\frac{hfs}{\varepsilon(\rho C_p)_f}(T_s-T_f), \quad (3)$$

$$0=\frac{k_s}{(\rho C_p)_s}\left(\frac{\partial^2 T_s}{\partial y^2}+\frac{\partial^2 T_s}{\partial x^2}\right)+\frac{hfs}{(1-\varepsilon)(\rho C_p)_s}(T_f-T_s), \quad (4)$$

$$\frac{1}{\varepsilon}\left[u\frac{\partial C}{\partial x}+v\frac{\partial C}{\partial y}\right]=D_m\left(\frac{\partial^2 C}{\partial y^2}+\frac{\partial^2 C}{\partial x^2}\right)+\frac{D_m k_T}{T_m}\frac{\partial^2 T_f}{\partial y^2} \quad (5)$$

According to the continuity Eq. (1), the magnitudes of inflow and outflow are equal. Eq. (2), is a momentum equation that upholds law of conservation of momentum. Inertial forces are responsible for foremost term on left hand side (LHS) of Eq. (2). In contrast, additional effects from porous media and an aligned magnetic field are responsible for the second-to-last term. Eq. (3) explains that heat can be transferred through a fluid using one of three methods, convection (LHS), and conduction (first term on RHS). The third term in RHS describes heat fluxes between the solid and liquid phases and the Dufour effect (second terms on RHS). The porous is matrix form and saturating fluid type are what decide the heat transfer coefficient for fluid hfs. The value of this coefficient has been determined after extensive experimental study. High values of hfs result in quick heat transfer between the phases, while low values of hfs result in relatively significant LTNE effects which are taken from the previous study [10, 19]. Eq. (5) is a representation of the mass transfer equation or the diffusion equation. RHS's final statement considers the Soret effect's added weight.

The boundary requirements are pertinent as $u,\ v$ are velocity components of moving fluid in x, y directions are given by

$$\left.\begin{aligned} u=U_w=cx, v=v_w, T_f=T_w, T_s=T_w, C=C_w \ at\ y=0, \\ u\to 0,\ T_f\to T_\infty, T_s\to T_\infty, C\to C_\infty\ as\ y\to\infty \end{aligned}\right\} \quad (6)$$

Where β is Casson parameter, ρ is Density of fluid (kg m^{-3}), $\alpha=\frac{k}{\rho C_p}$ is thermal diffusivity (m^{2}s^{-1}), k is thermal conductivity (W m^{-1} K^{-1}), C_p is heat capacity (J Kg^{-1} K^{-1}), , μ is dynamic viscosity (kg m^{-1} s^{-1}), σ is electrical conductivity, ν_f is kinematic viscosity (m^{2}s^{-1}), ε is porosity, C_∞ is ambient Concentration, C is Concentration of fluid, C_w is wall Concentration, T_∞ is ambient temperature (K), T_f is fluid temperature (K), T_s is solid temperature (K), T_w is wall temperature (K), K' is permeability of porous medium.

The similarity transformations are applied in above model with stream function Ψ, and similarity variable η with velocity profile $f'(\eta)$, temperature profiles for both fluid $\theta_f(\eta)$, solid $\theta_s(\eta)$ phases respectively and $\chi(\eta)$ concentration profile are taken as follows:

$$\left.\begin{aligned} \Psi=\sqrt{cv_f}\,xf(\eta),\ \eta=\sqrt{\frac{c}{v_f}}y, \\ u=\frac{\partial\Psi}{\partial y}=cxf'(\eta),\ v=-\frac{\partial\Psi}{\partial x}=-\sqrt{cv_f}\,f(\eta), \\ \theta_f(\eta)=\frac{T_f-T_\infty}{T_w-T_\infty},\ \theta_s(\eta)=\frac{T_s-T_\infty}{T_w-T_\infty}, \chi(\eta)=\frac{C-C_\infty}{C_w-T_\infty} \end{aligned}\right\} \quad (7)$$

Eq. (7) is used to decrease the governing Eq. (1) – (5), which are given by:

$$(1+\tfrac{1}{\beta})f'''(\eta)-\tfrac{1}{\epsilon^2}[f'^2(\eta)-f(\eta)f''(\eta)]-Kf'(\eta)-MSin^2\emptyset f'(\eta)=0 \quad (8)$$

$$\frac{1}{Pr}\theta''_f(\eta)+\frac{1}{\epsilon}f(\eta)\,\theta'_f(\eta)+Du\chi"(\eta)+H(\theta_s(\eta)-\theta_f(\eta))=0 \quad (9)$$

$$\frac{1}{Pr}\,\theta''_s(\eta) + \gamma H(\theta_f(\eta) - \theta_s(\eta)) = 0 \tag{10}$$

$$\frac{1}{Sc}\chi"(\eta) + \frac{1}{\epsilon}f(\eta)\chi'(\eta) + Sr\,\theta"_f(\eta) = 0 \tag{11}$$

Moreover, reduced boundary conditions,

$$\left.\begin{aligned} f'(0) = 1, f(0) = \kappa\chi'(0), \theta_f(0) = 1, \theta_s(0) = 1, \chi(0) = 1, as\ \eta \to 0\ , \\ f'(\infty) \to 0, \theta_f(\infty) \to 0,\ \theta_s(\infty) \to 0,\ \chi(\infty) \to 0, as\ \eta \to \infty \end{aligned}\right\} \tag{12}$$

Here, $V_w = -\kappa\sqrt{(cv_f)}\chi'(0)$ denotes the wall blowing velocity and κ(≥ 0) the Stefan blowing parameter resulting from mass transfer taken from previous work Fang *et al.,* [39].
Where, the following are the non-dimensional parameters defined as aligned Magnetic parameter M, Porosity parameter K, Prandtl number Pr, Dufour number Du, Soret number Sr, Schmidt number Sc, Conductivity ratio of modified Porosity or porosity ratio γ, Heat transfer parameter H are defined by,

$$\left.\begin{aligned} M = \frac{\sigma_f {B_0}^2}{\rho_f c}, K = \frac{v_f}{K'c}, Pr = \frac{v_f}{\alpha_f}, Du = \frac{D_m K_T(C_w - C_\infty)}{v_f C_s C_p(T_w - T_\infty)}, Sr = \frac{D_m K_T(T_w - T_\infty)}{v_f T_m(C_w - C_\infty)} \\ Sc = \frac{v_f}{D_m}, \gamma = \frac{\varepsilon k_f}{(1-\varepsilon)k_s}, H = \frac{(hfs)\alpha_f}{\varepsilon c k_f} \end{aligned}\right\} \tag{13}$$

With C_s – Concentration susceptibility of Solid, D_m – Mass Diffusivity, K_T - Thermal diffusion ratio, T_m – Mean value of temperature (K).

The Nusselt numbers, *Nu$_f$* - Nusselt number for fluid phase, *Nu$_s$* - Nusselt number for solid phase, local Skin Friction C_f and Sherwood number Sh are employed to compute flow resistance, rate of mass and heat transfer. The relationship of these numbers in their non-dimensional form are organised with local Reynolds number *Re* as follows:

$$Re^{-\frac{1}{2}}Nu_f = (-\theta'_f(0)) \tag{14}$$

$$Re^{-\frac{1}{2}}Nu_s = (-\theta'_s(0)) \tag{15}$$

$$Re^{\frac{1}{2}}C_f = 2\left(1 + \frac{1}{\beta}\right)f''(0) \tag{16}$$

$$Re^{-\frac{1}{2}}Sh = (-\chi'(0)) \tag{17}$$

3. Numerical Analysis

Runge-Kutta-4 with shooting technique is used to numerically solve ODEs subject to specific boundary conditions, enabling the study of dynamic systems and phenomena that cannot be easily solved analytically.

Therefore, by using this numerical method, we analyze the flow model for solving ODEs from Eq. (8) through Eq. (11) with appropriate boundary conditions Eq. (12) over a range of values of admissible parameters in Eq. (13) $M, K, Pr, Du, Sr, Sc\ and\ H$. The boundary value problem has been transformed into initial value problem by using $f = f_1, f' = f_2, f'' = f_3,\ \theta_f = f_4,\ \theta'_f = f_5,\ \theta_s = f_6,\ \theta'_s = f_7, \chi = f_8, \chi' = f_9$. Consequently, the equations are transformed into,

$$f_1' = f_2,$$

$$f_2' = f_3,$$
$$f_3' = -\left(\frac{-\frac{1}{\epsilon^2}[f_2^2 - f_1 f_3] - K f_2 - MSin^2\emptyset f_2}{\left(1+\frac{1}{\beta}\right)}\right),$$
$$f_4' = f_5,$$
$$f_5' = -Pr\left(\frac{1}{\epsilon} f_1 f_5 + Du f_9' + H(f_6 - f_4)\right),$$
$$f_6' = f_7,$$
$$f_6' = f_7,$$
$$f_7' = -Pr\gamma H(f_4 - f_6),$$
$$f_8' = f_9,$$
$$f_9' = -Sc\left(\frac{1}{\epsilon} f_1 f_9 + Sr f_5'\right),$$

The reduced boundary conditions are follows:

$$f_2(0) = 1, f_1(0) = \kappa f_9(0), f_4(0) = 1, f_6(0) = 1, f_8(0) = 1,$$
$$f_2(\infty) \to 0, f_4(\infty) \to 0, f_6(\infty) \to 0, f_8(\infty) \to 0.$$

A finite domain $0 \leq \eta \leq \eta_\infty$ is required for the RK process. Selecting the appropriate ∞ value for the present model requires consideration of values of pertinent parameters. Moreover, η_∞ is treated as less than 10 in this instance. After the convergence requirement is satisfied, reduced ordinary differential equations are solved with given set of parameters using RK-4 procedure with shooting technique, to obtain the absolute precision. The above-mentioned steps are repeated until the obtained results satisfy the convergence criterion by attaining preferred accuracy level of 10^{-6}.

4. Results and Discussion

In this case. similarity solution is used to create numerical solutions for the current problem for all thermophysical parameter values influencing dynamics of the fluid in the flow regime. LTNE conditions are used to compare and compute the Casson fluid flow, mass, and heat transfer characteristics on stretched sheet. Soret and Dufour effect as well as the aligned magnetic field effect are taken into consideration during modelling. The impacts of non-dimensional elements are visually represented under the flow assumptions. The Prandtl number, Pr has been fixed in order to examine how the parameters affect velocity, mass, and heat transmission. Validation of the method has been taken for different values of Pr. The numerical results in Table 1 for present study were also compared to published research, and we noticed that they made a convincing case.

Table 1
Comparison for $\theta_f'(0)$ & $\theta_s'(0)$ for different values of Prandtl number Pr

$\boldsymbol{Pr}$	Prakash *et al.,* [5]		Alhadhrami *et al.,* [2]		Present Study	
	$\boldsymbol{\theta_f'(0)}$	$\boldsymbol{\theta_s'(0)}$	$\boldsymbol{\theta_f'(0)}$	$\boldsymbol{\theta_s'(0)}$	$\boldsymbol{\theta_f'(0)}$	$\boldsymbol{\theta_s'(0)}$
0.7	0.808570	0.808578	0.808624	0.808628	0.808678	0.808726
1.0	0.999927	0.999937	0.999948	0.999957	0.999967	0.999979
2.0	1.923556	1.923573	1.923678	1.923689	1.923795	1.923813
10	3.720444	3.720475	3.720619	3.720635	3.720794	3.720811

The aligned magnetic parameter M sluggish movement on velocity profile $f'(\eta)$ is depicted in Figure 2(a), where $f'(\eta)$ declines as the M value increases. The movement of the liquid is slowed down when aligned magnetism is present in the flow area. The Lorentz force, is a resistive force

created by a transverse magnetic field as a result of cumulative M, is coupled to the lowered velocity $f'(\eta)$ in this case. The Lorentz force, which frequently opposes the flow, is produced by a rise in aligned magnetic parameter M and causes velocity boundary layer thickness to decrease. The Lorentz force that is created, cause the liquid's velocity $f'(\eta)$, to decrease. It is shown in Figure 2(b) how aligned magnetic parameter M affects the value of temperature profile $\theta_f(\eta)$. In this case, as M increases, the fluid phase's temperature increases. These experiments indicate that the second layer of resistance added by the aligned magnetic force causes the stream to slow down and get hotter. Here, thermal energy is dissipated by moving the fluid at a base liquid velocity in direction of aligned magnetic field action. This increases $\theta_f(\eta)$ by warming the liquid.

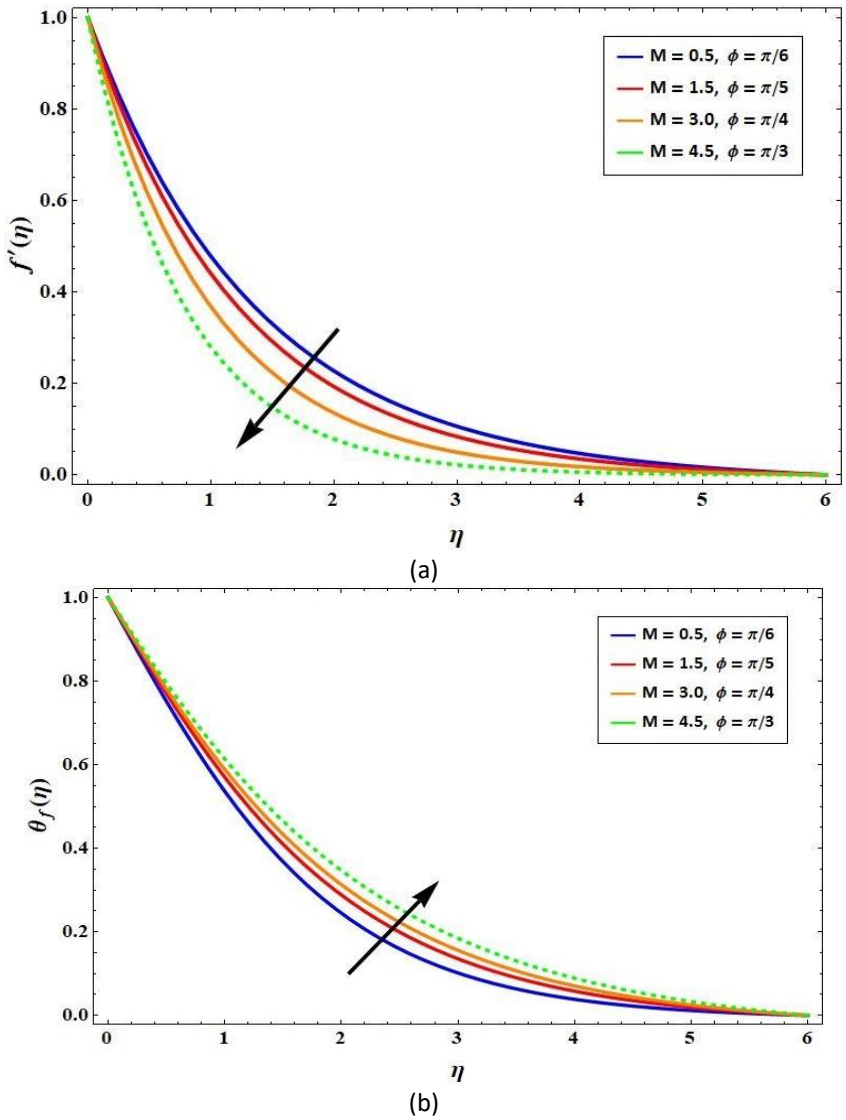

Fig. 2. (a) Variation of aligned magnetic parameter M on velocity profile $f'(\eta)$ (b) Variation of aligned magnetic parameter M on temperature profile $\theta_f(\eta)$

Figure 3(a) exerts influence on porosity parameter K on velocity profile $f'(\eta)$. The advanced K values decline $f'(\eta)$. The permeable zone's resistive power and mean absorption coefficient both fall, which lowers the velocity, $f'(\eta)$. When the porousness is large, there is more room for the fluid to move. The amount of space for the liquid to move reduces as a material's porosity decreases. Consequently, velocity declines.

In Figure 3(b), activation of K on $\theta_f(\eta)$ is demonstrated. The $\theta_f(\eta)$ increases along with the increase in K. The increment in K causes liquid to become more viscous and because of the higher viscosity, which regulates liquid travel across surfaces, the liquid's velocity decays. This is consistent with the idea that when K increases, more stress is produced, enhancing thickness of thermal boundary layer.

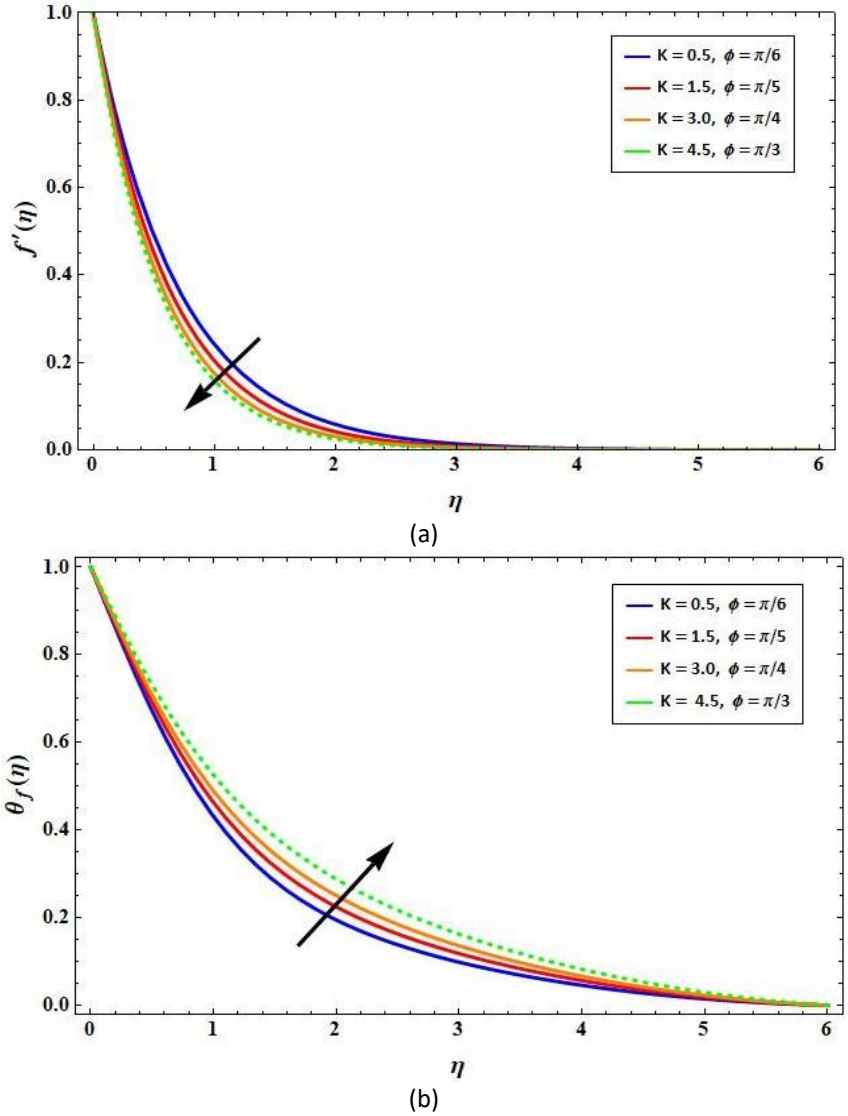

Fig. 3. (a) Varied values of porosity parameter K on velocity profile f'(η)
(b) Varied values of porosity parameter K on temperature profile $\theta_f(\eta)$

Figures 4(a) and 4(b) shows Casson parameter β effect on velocity profile $f'(\eta)$ which decreases, despite the fact that temperature profile $\theta_f(\eta)$ shows the opposite tendency. The heat transfer coefficient rises as values of β increase, and the fluid's viscosity advances. When the Casson parameter β raised, the velocity field is suppressed (here fluid acts as Newtonian fluid due to raise in Casson parameter), as a result, temperature $\theta_f(\eta)$ increases and velocity $f'(\eta)$ degrades with an increase in β.

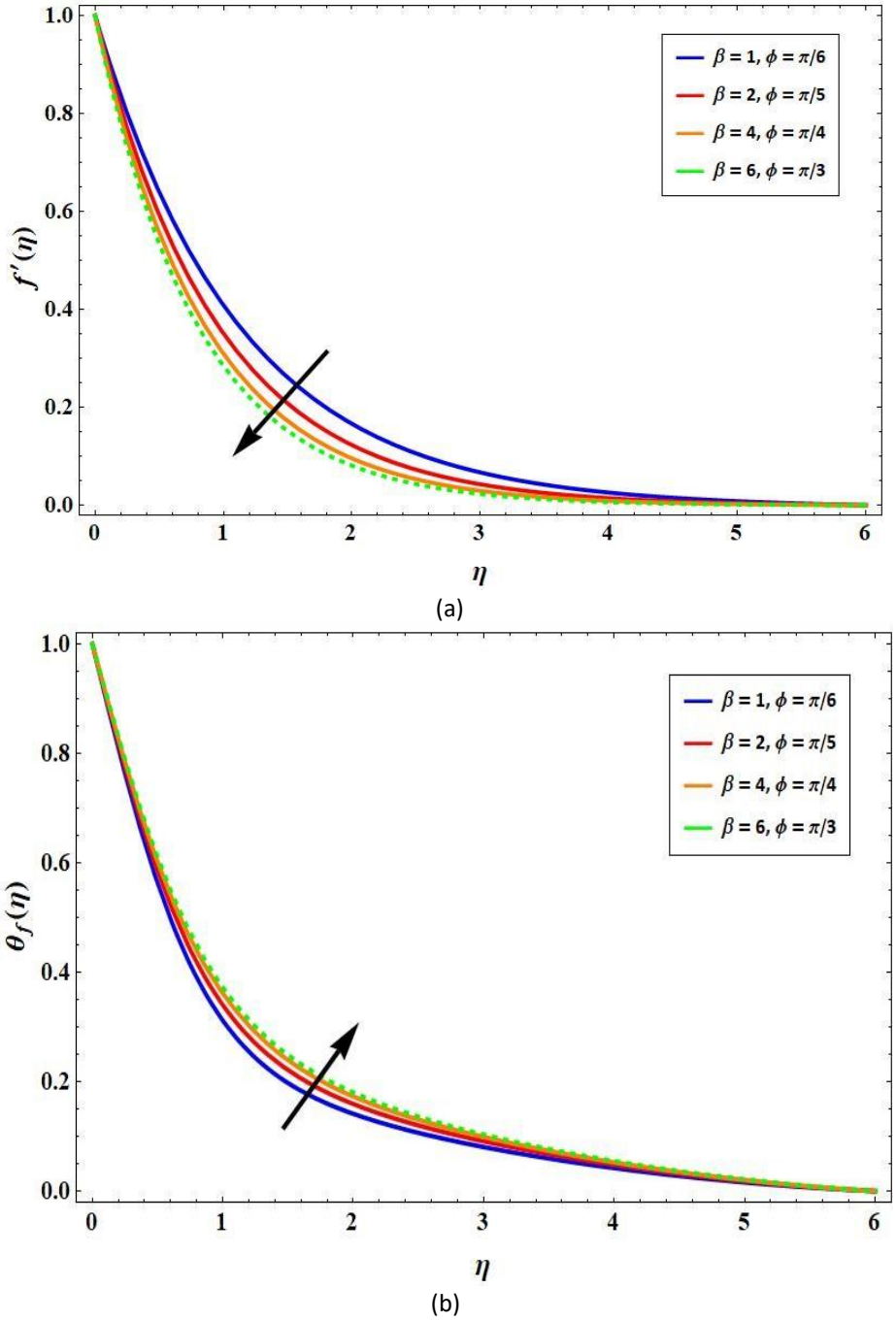

Fig. 4. (a) Varied values of Casson parameter β on velocity profile f'(η) (b) Varied values of Casson parameter β on temperature profile $\theta_f(\eta)$

Figures 5(a) and 5(b) depict, impact of blowing parameter κ on $f'(\eta)$ and $\chi(\eta)$. Increasing κ, blowing parameter value, both $f'(\eta)$ and $\chi(\eta)$ are augmented and blown farther from the wall with thicker boundary layer and meanwhile variance of the concentration profile grows with raise in blowing parameter κ.

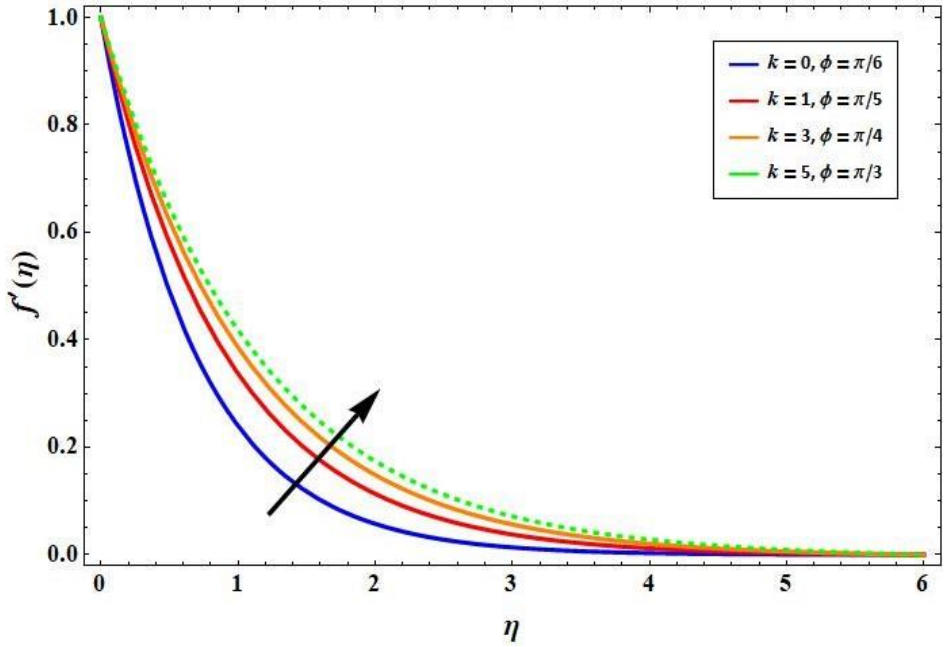

(a)

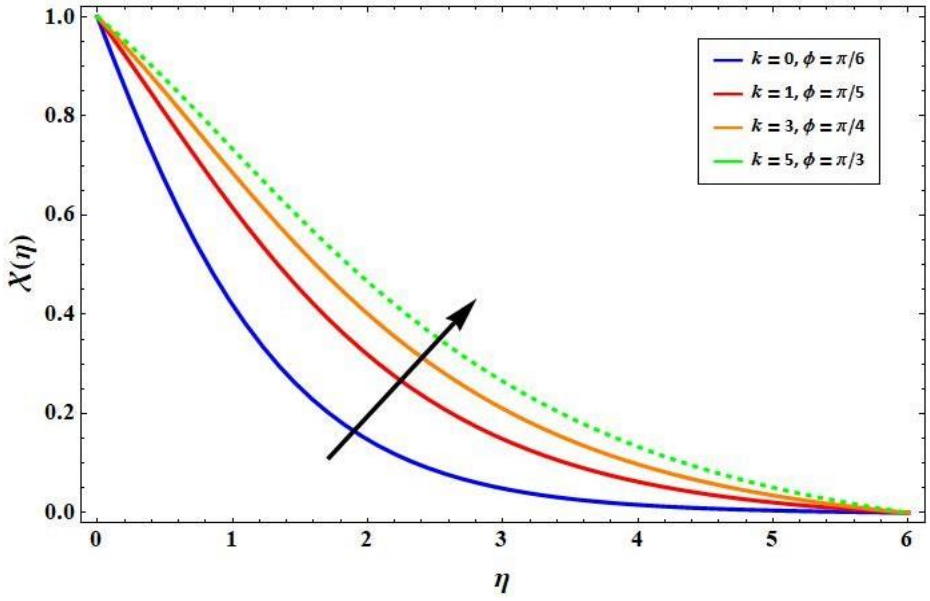

(b)

Fig. 5. (a) Varied values of Stefan blowing parameter κ on velocity profile f'(η)
(b) Varied values of Stefan blowing parameter κ on concentration profile $\chi(\eta)$

The significant effects of porosity ratio γ on both temperature profiles $\theta_f(\eta)$ and $\theta_s(\eta)$ are depicted in Figures 6(a) and 6(b). Growing γ causes both these profiles $\theta_f(\eta)$ and $\theta_s(\eta)$ to decline. Physically, convection γ can be completely supressed for higher levels, which causes both profiles $\theta_f(\eta)$ and $\theta_s(\eta)$ to decelerate.

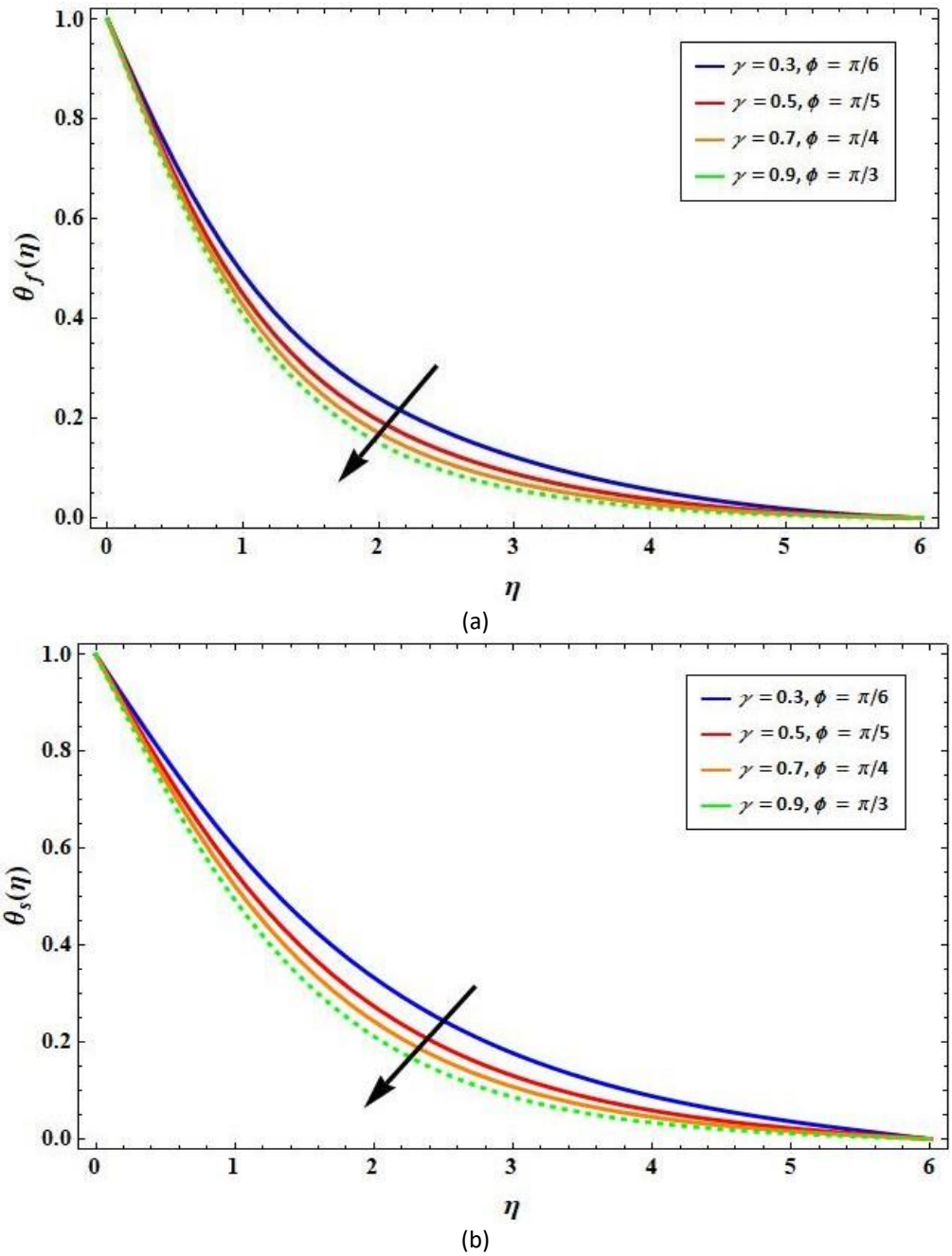

Fig. 6. (a) Varied values of porosity ratio γ on temperature profile fluid phase $\theta_f(\eta)$ (b) Varied values of porosity ratio γ on temperature profile solid phase $\theta_s(\eta)$

Soret and Dufour effects are both accounted in the energy equation. Soret effect is a temperature gradient-induced mass flow, whereas, Dufour effect is an enthalpy flux brought on by concentration. The effect of Dufour number, Du on both phases of temperature profiles $\theta_f(\eta)$ and $\theta_s(\eta)$ is shown in Figures 7(a) and 7(b). Both profiles $\theta_f(\eta)$ and $\theta_s(\eta)$ are improved by the expanding Du value

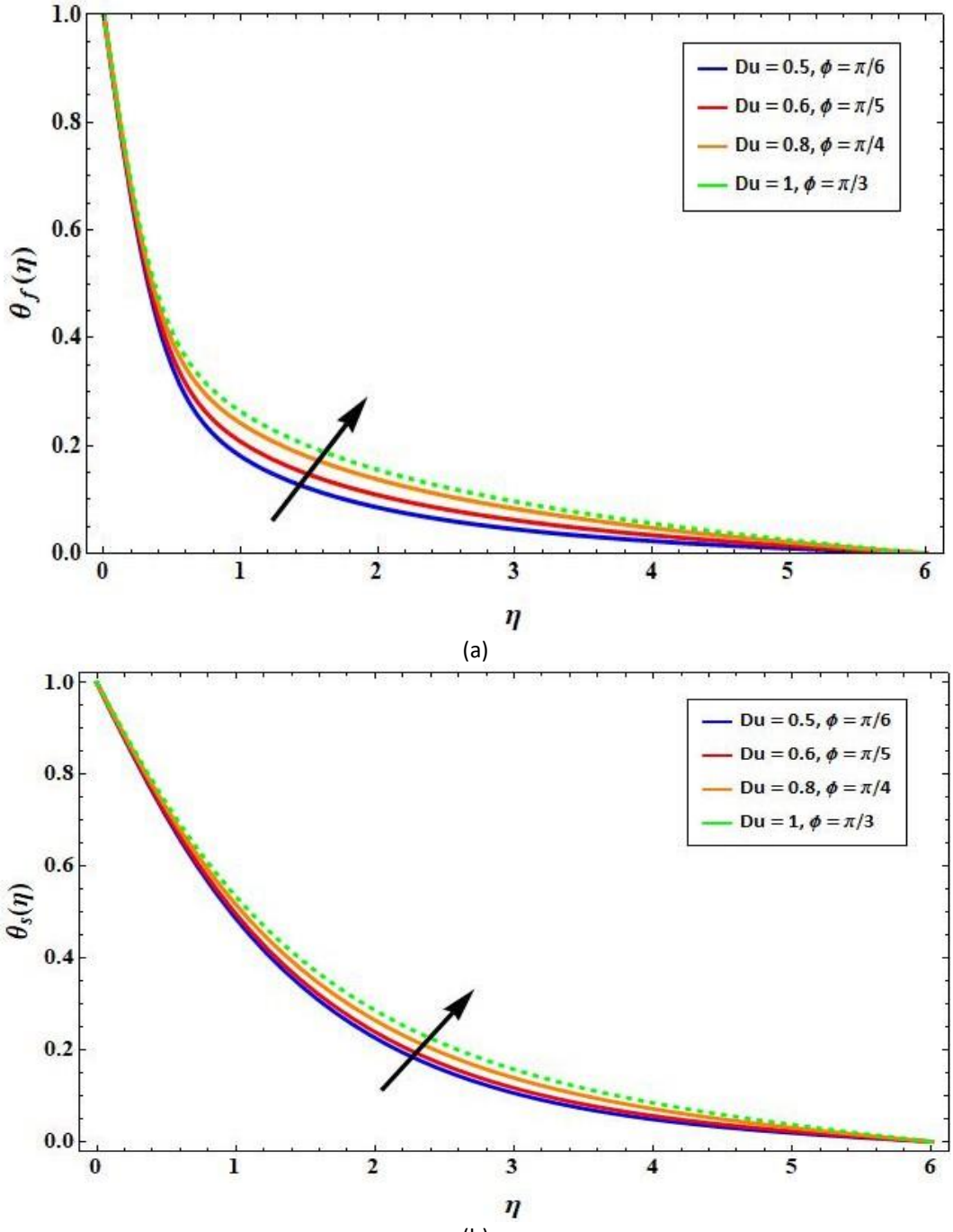

Fig. 7. (a) Varied values of Dufour number Du on temperature profile fluid phase $\theta_f(\eta)$ (b) Varied values of Dufour number Du on temperature profile solid phase $\theta_s(\eta)$

Figures 8(a) and 8(b) show stimulation of heat transfer parameter H in temperature profiles for both phases $\theta_f(\eta)$ and $\theta_s(\eta)$ respectively. Although the $\theta_f(\eta)$ increases but $\theta_s(\eta)$ decreases due to growth in H. The quick rate of heat transfer between both phases causes $\theta_s(\eta)$ to fall, while $\theta_f(\eta)$ rises.

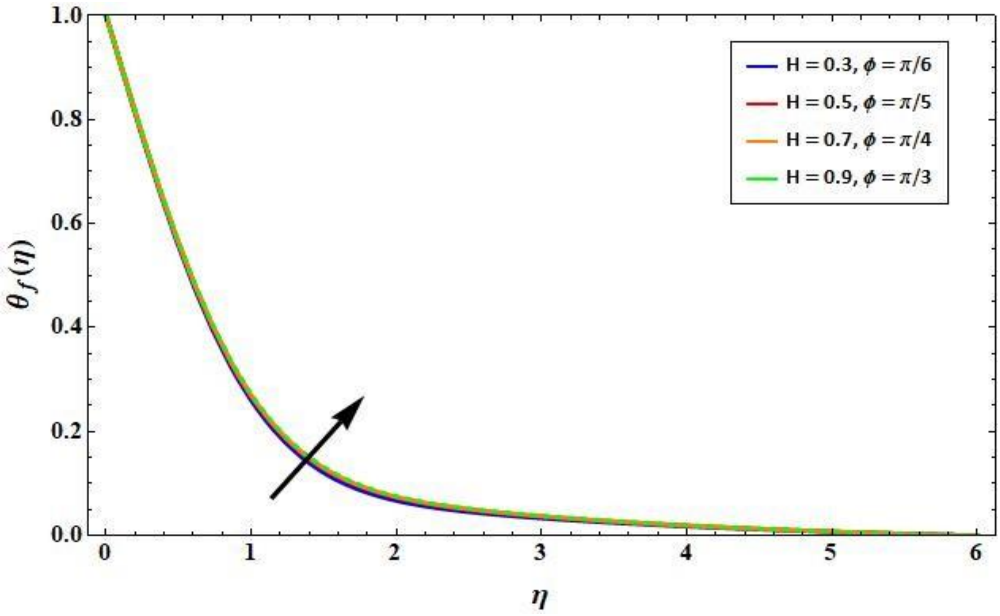

(a)

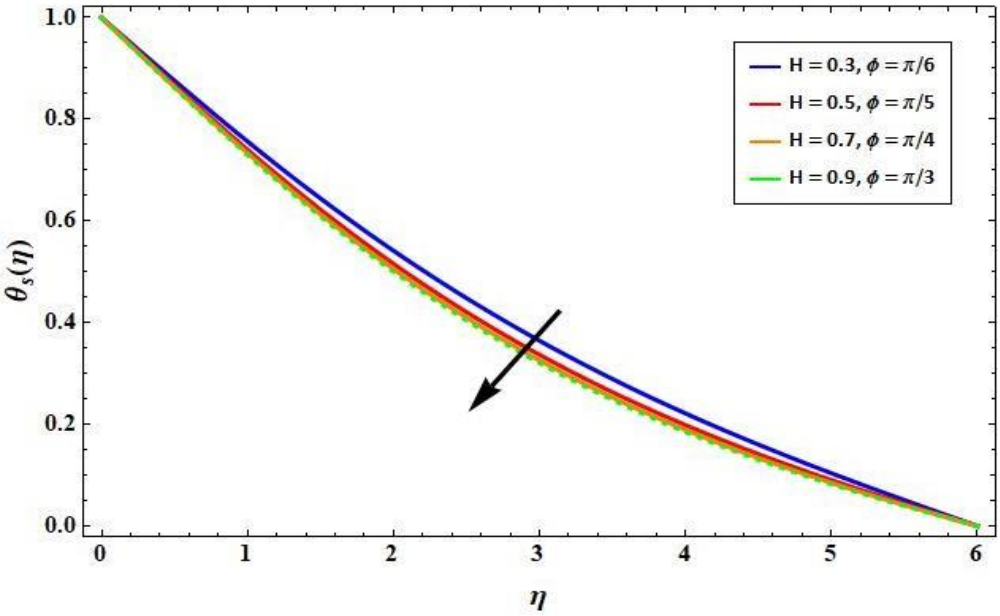

(b)

Fig. 8. (a) Varied values of heat transfer parameter H on temperature profile fluid phase $\theta_f(\eta)$ (b) Varied values of heat transfer parameter H on temperature profile fluid phase $\theta_s(\eta)$

The comparison of temperature profiles for fluid $\theta_f(\eta)$ and for solid $\theta_s(\eta)$ phases for Casson fluid under the influence of heat transfer parameter H is seen in Figure 9(a). The increasing in H, heat transfer rate in both the phases as shown in the graph, specifies that the structure is endeavoring to adjust the LTNE phase. $\theta_f(\eta)$ and $\theta_s(\eta)$ for both phases differ significantly for H values in the middle of the range. In this instance, we may claim that the LTNE is impacting the flow. When H is increased, the structure enters thermal equilibrium, and although if the discrepancy is still present, the fluid phase progressively changes into the solid phase. When H increases, the effects of LTE are ultimately felt by the structure, and they are fully realized when $\theta_f(\eta)$ and $\theta_s(\eta)$ are nearly equal. The comparison of temperature profiles for both phases $\theta_f(\eta)$ and $\theta_s(\eta)$ for Casson fluid under the

influence of porosity ratio γ shown in Figure 9(b). In this case, as shown in the graph, the γ value when raised indicates that structure is attempting to transform LTE phase.

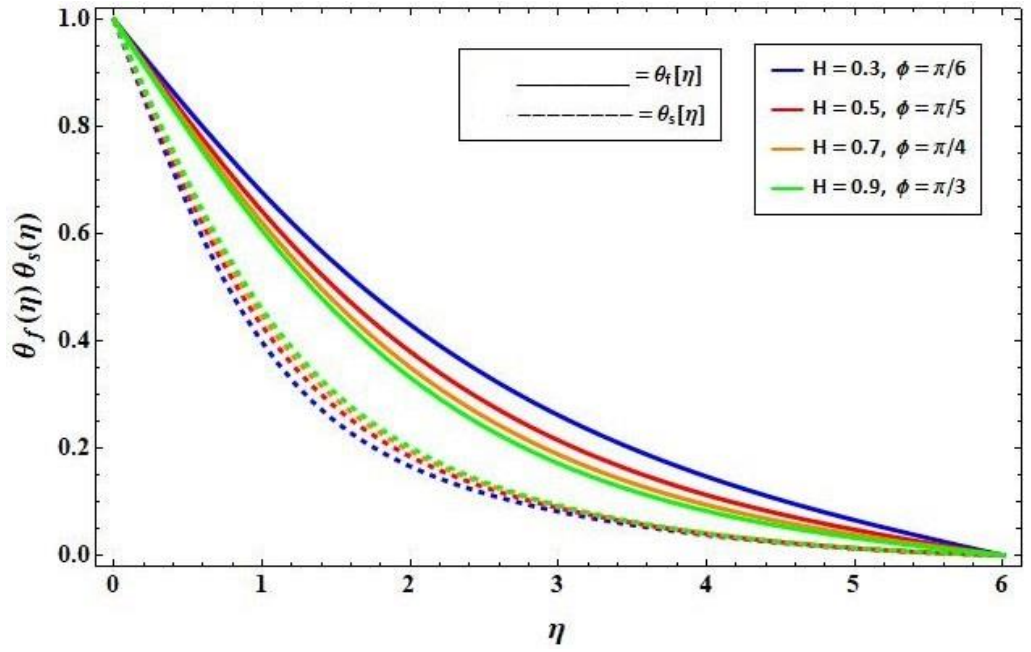

(a)

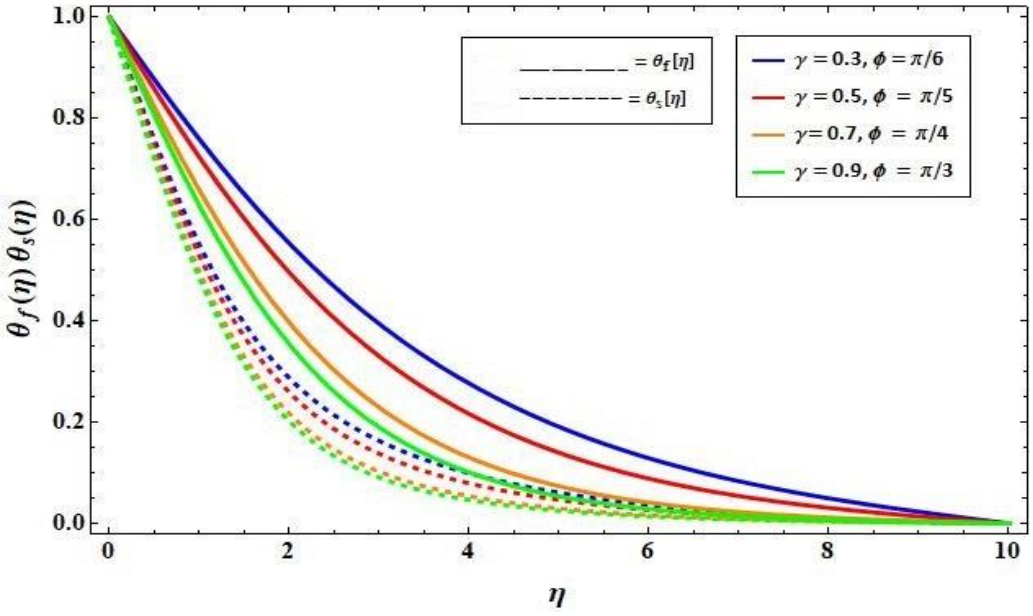

(b)

Fig. 9. (a) Comparison of $\theta_f(\eta)\theta_s(\eta)$ for various values of heat transfer parameter H (b) Comparison of $\theta_f(\eta)\theta_s(\eta)$ for various values of heat transfer parameter γ

In Figure 10(a), the stimulation of Sr on concentration profile $\chi(\eta)$ is depicted. An increase in Soret number Sr enhances concentration profile $\chi(\eta)$. Relationship between concentration and temperature changes can be used to calculate the Sr. Higher Sr diffuse species encourage mass transfer. In Figure 10(b), effect of Schmidt number Sc over concentration profile $\chi(\eta)$ is represented. As the Sc increases, the $\chi(\eta)$ declines. This is explained by the proportion of mass to momentum diffusivities. The high viscous diffusion of progressive Sc values speed up molecule motion.

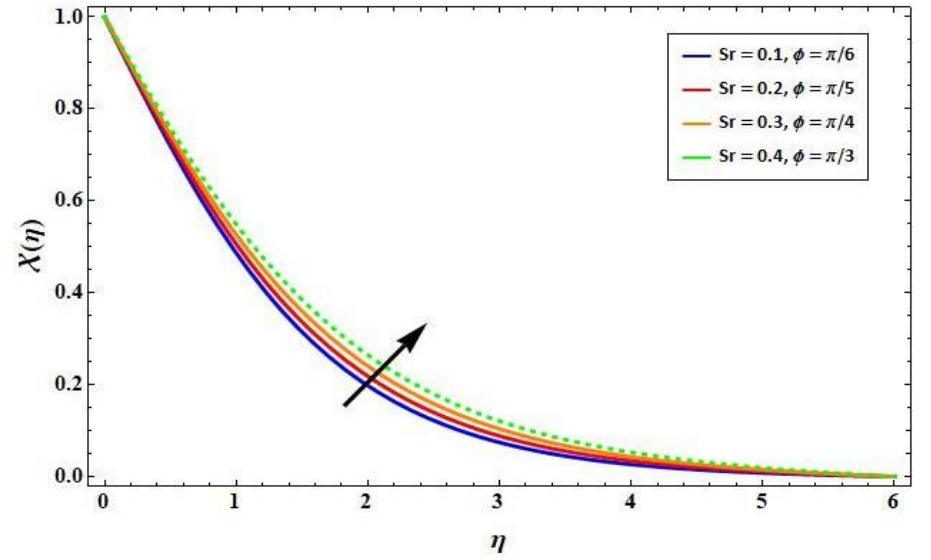

(a)

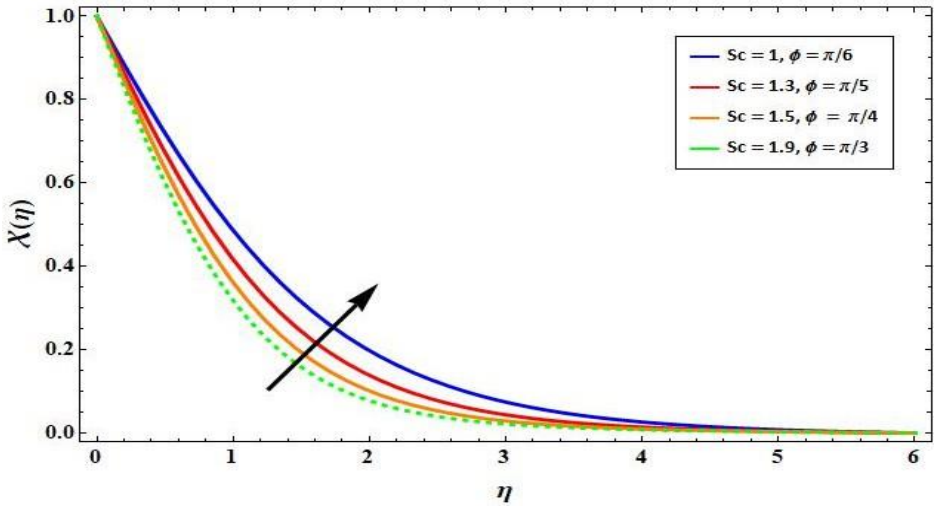

(b)

Fig. 10. (a) Varied values of Soret number Sr on concentration profile $\chi(\eta)$ (b) Varied values of Schmidt number Sc on concentration profile $\chi(\eta)$

In Figures 11(a) and 11(b) levering of Soret number Sr and Stefan blowing parameter κ on Sherwood number $Re^{-1/2}\,Sh$ verses Schmidt number Sc are shown. As these numbers, Sr and κ values are raised, which causes $Re^{-1/2}\,Sh$ to decline. Also, $Re^{-1/2}\,Sh$ is further advanced by raise in Sc values.

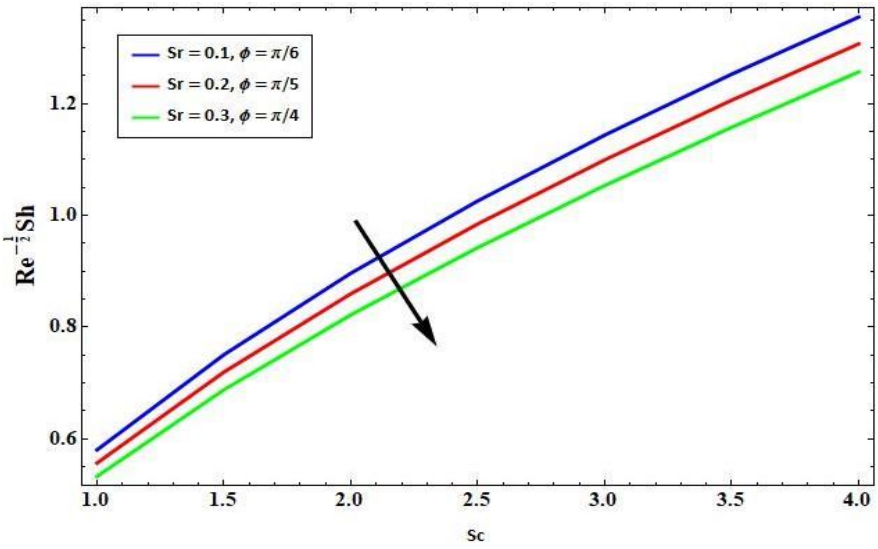

(a)

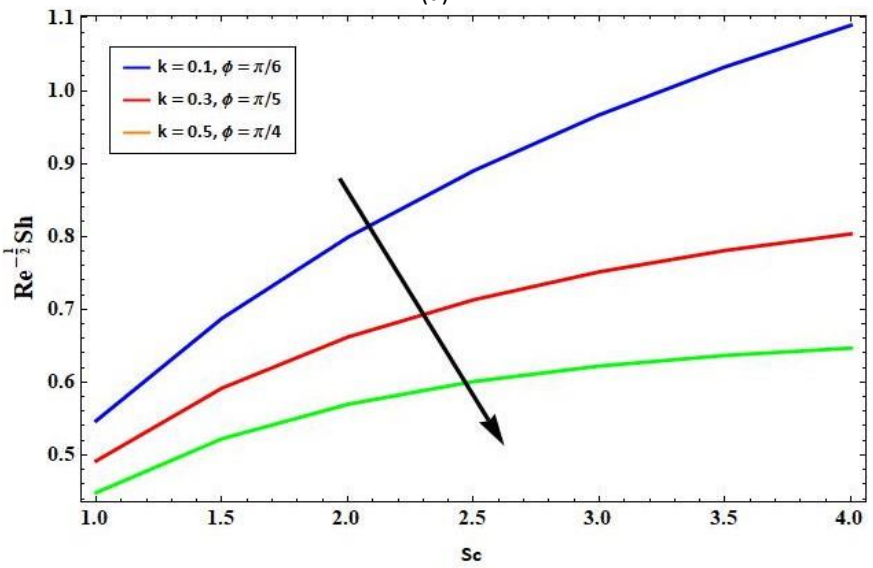

(b)

Fig. 11. (a) Effects of Sherwood number $Re^{-1/2}\,Sh$ verses Sc for various values of Soret number Sr (b) Effects of Sherwood number $Re^{-1/2}\,Sh$ verses Sc for various values of Stefan blowing parameter κ

Figures 12(a) and 12(b) show how aligned magnetic parameter M and Casson parameter β are levered on skin friction number $Re^{\frac{1}{2}}\,C_f$ in comparison to porosity parameter K and Stefan blowing parameter κ, respectively. Skin friction $Re^{\frac{1}{2}}\,C_f$ gets better as β value increases, whereas when M value increases it shows the reverse effect. Increasing K and κ values also refine the skin friction.

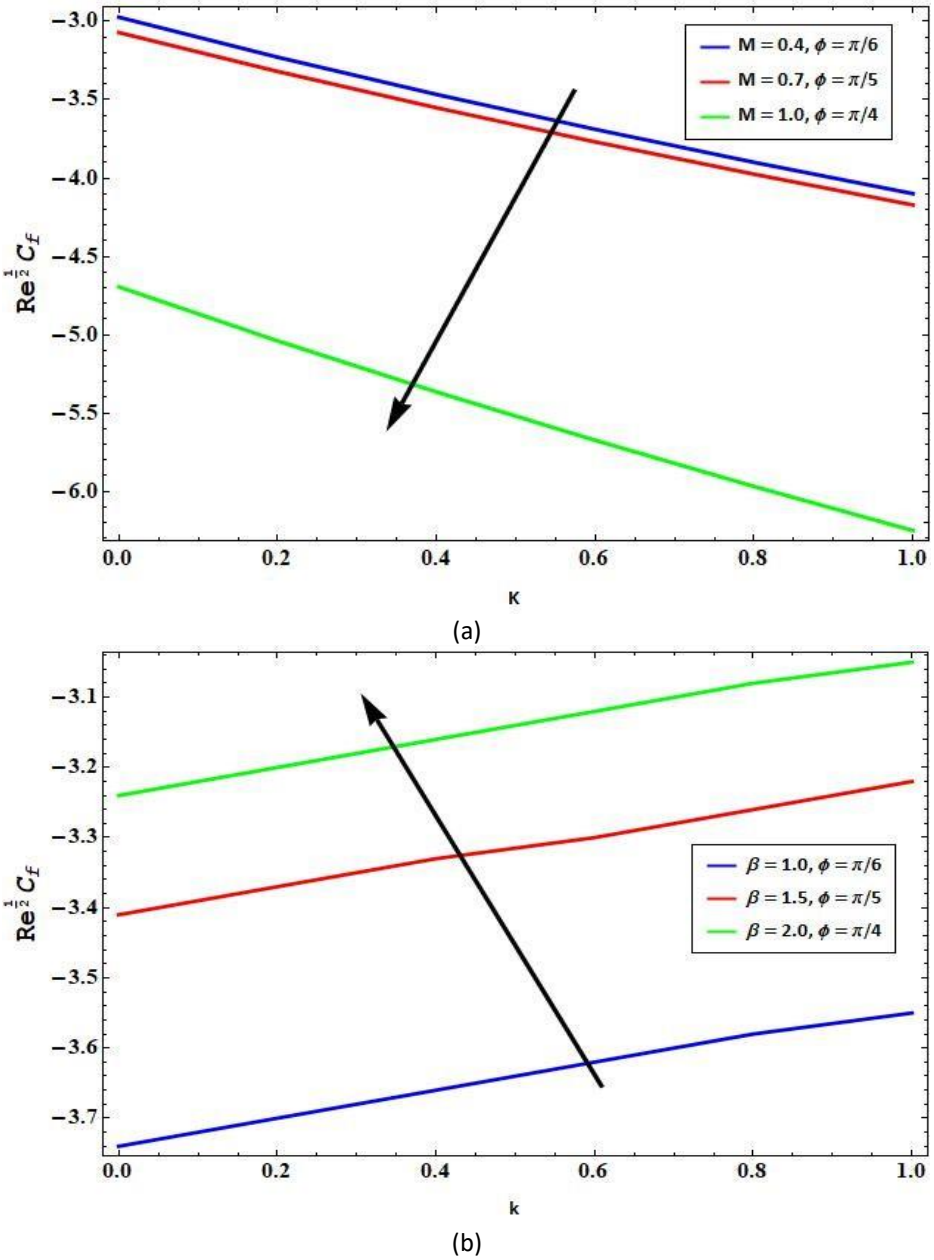

Fig. 12. (a) Effects of skin friction $Re^{\frac{1}{2}}C_f$ verses K for various values of aligned magnetic parameter M (b) Effects skin friction $Re^{\frac{1}{2}}C_f$ verses κ for various values of Casson parameter β

Levering on Dufour number Du on Nusselt numbers for both fluid and solid $Re^{-\frac{1}{2}}Nu_f$ and $Re^{-\frac{1}{2}}Nu_s$ versus Porosity ratio γ is shown in Figures 13(a) and 13(b). The Nusselt numbers for both phases $Re^{-\frac{1}{2}}Nu_f$ and $Re^{-\frac{1}{2}}Nu_s$ drop as a result of Du rising values. Additionally, increasing values of porosity ratio γ enhance both $Re^{-\frac{1}{2}}Nu_f$ and $Re^{-\frac{1}{2}}Nu_s$ these numbers.

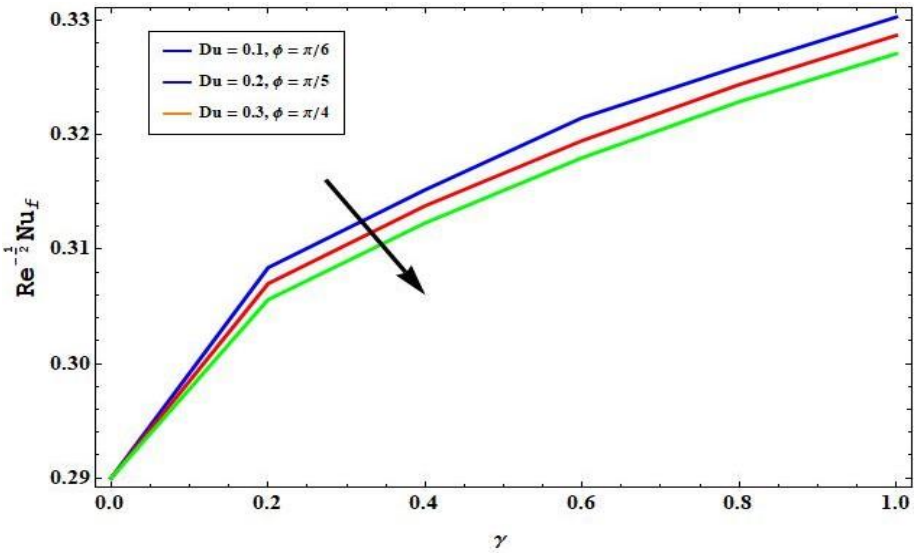

(a)

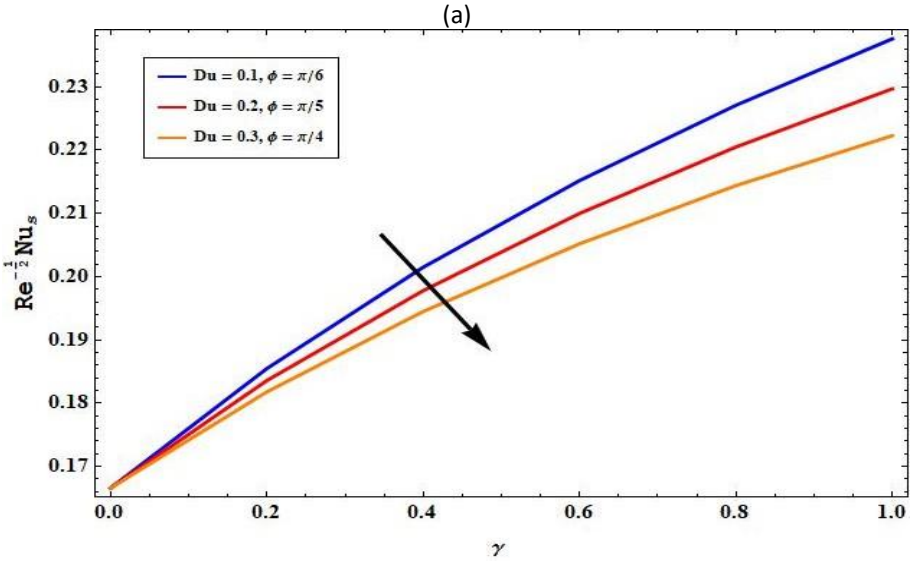

Fig. 13. (a) Effects of Nusselt number $Re^{-\frac{1}{2}}Nu_f$ for liquid phase verses porosity ratio γ for various values of Dufour number Du (b) Effects of Nusselt number $Re^{-\frac{1}{2}}Nu_s$ for solid phase verses porosity ratio γ for various values of Dufour number Du

5. Conclusions

Current inquiry focuses on impact of aligned magnetic field, Stefan Blowing parameter, Soret and Dufour effects on behaviour of Casson fluid across two-dimensional stretching sheet in a porous material as well as LTNE conditions. The influence of non-dimensional characteristics is depicted graphically under the stated flow assumptions. The present study demonstrates that;

i. The temperature profile $\theta_f(\eta)$ improves, while the velocity profile $f'(\eta)$ decreases as aligned magnetic parameter M value increases due to retarding Lorentz force.
ii. The increase in porosity parameter K values reduces velocity profile $f'(\eta)$ due to decrease in the mean absorption coefficient, while enhancing temperature profile (liquid) $\theta_f(\eta)$.
iii. The temperature profiles of both phases $\theta_f(\eta)$ and $\theta_s(\eta)$ decline with increase in porosity modified conductivity ratio γ values,

iv. Incremental values of Du exhibit improvement in temperature profiles of both phases $\theta_f(\eta)$ and $\theta_s(\eta)$.
v. The concentration profile $\chi(\eta)$ is boosted by rising the values of Sr as Soret number promotes mass transport and $\chi(\eta)$ falls when there is a rise in Sc values as progressive Schmidt number shown high viscous diffusion which decelerates molecular movements.
vi. Both liquid and solid matrix phases transmit heat more quickly when Du value increases, leading to the influence of concentration gradients on temperature profiles and vice-versa.

Acknowledgement
This research was not funded by any grant.

References

[1] Reddy, J. V., V. Sugunamma, and N. Sandeep. "Effect of aligned magnetic field on Casson fluid flow past a vertical oscillating plate in porous medium." *Journal of Advanced Physics* 5, no. 4 (2016): 295-301. https://doi.org/10.1166/jap.2016.1267
[2] Kumar, K. Kranthi, C. H. Baby Rani, and A. V. Papa Rao. "MHD Casson Fluid Flow along Inclined Plate with Hall and Aligned Magnetic Effects." *Frontiers in Heat and Mass Transfer (FHMT)* 17 (2021). http://dx.doi.org/10.5098/hmt.17.2
[3] Saravana, R., M. Sailaja, and R. Hemadri Reddy. "Effect of aligned magnetic field on Casson fluid flow over a stretched surface of non-uniform thickness." *Nonlinear Engineering* 8, no. 1 (2019): 283-292. https://doi.org/10.1515/nleng-2017-0173
[4] Reddy, B. Mahesh. "Aligned magnetic field effect on Casson fluid flow over a non-uniform thickness stretched surface." *Int J Multidiscip Edu Res* 9, no. 12 (2020): 5.
[5] Kodi, Raghunath, and Obulesu Mopuri. "Unsteady MHD oscillatory Casson fluid flow past an inclined vertical porous plate in the presence of chemical reaction with heat absorption and Soret effects." *Heat Transfer* 51, no. 1 (2022): 733-752. https://doi.org/10.1002/htj.22327
[6] Nield, Donald A., and Adrian Bejan. *Convection in porous media*. Vol. 3. New York: springer, 2006.
[7] Alhadhrami, A., C. S. Vishalakshi, B. M. Prasanna, B. R. Sreenivasa, Hassan AH Alzahrani, RJ Punith Gowda, and R. Naveen Kumar. "Numerical simulation of local thermal non-equilibrium effects on the flow and heat transfer of non-Newtonian Casson fluid in a porous media." *Case Studies in Thermal Engineering* 28 (2021): 101483. https://doi.org/10.1016/j.csite.2021.101483
[8] Pati, Sukumar, Abhijit Borah, Manash Protim Boruah, and Pitambar R. Randive. "Critical review on local thermal equilibrium and local thermal non-equilibrium approaches for the analysis of forced convective flow through porous media." *International Communications in Heat and Mass Transfer* 132 (2022): 105889. https://doi.org/10.1016/j.icheatmasstransfer.2022.105889
[9] Muthtamilselvan, M., D. Prakash, and Deog-Hee Doh. "Effect of thermal non-equilibrium on transient hydromagnetic flow over a moving surface in a nanofluid saturated porous media." *Journal of Mechanical Science and Technology* 28 (2014): 3709-3718. https://doi.org/10.1007/s12206-014-0832-9
[10] Prakash, D., M. Muthtamilselvan, and Xiao-Dong Niu. "Unsteady MHD non-Darcian flow over a vertical stretching plate embedded in a porous medium with thermal non-equilibrium model." Advances in Applied Mathematics and Mechanics 8, no. 1 (2016): 52-66. https://doi.org/10.4208/aamm.2014.m462
[11] Vaddemani, Ramachandra Reddy, Raghunath Kodi, and Obulesu Mopuri. "Characteristics of MHD Casson fluid past an inclined vertical porous plate." *Materials Today: Proceedings* 49 (2022): 2136-2142. https://doi.org/10.1016/j.matpr.2021.08.328
[12] Sama, Nazrul Azlan Abdul, Norfifah Bachok, and Norihan Md Arifin. "The Significant Effect of Hydromagnetic on Carbon Nanotubes Based Nanofluids Flow and Heat Transfer Past a Porous Stretching/Shrinking Sheet." *Journal of Advanced Research in Fluid Mechanics and Thermal Sciences* 106, no. 1 (2023): 51-64. https://doi.org/10.37934/arfmts.106.1.5164
[13] Mahat, Rahimah, Sharidan Shafie, and Fatihhi Januddi. "Numerical analysis of mixed convection flow past a symmetric cylinder with viscous dissipation in viscoelastic nanofluid." *CFD letters* 13, no. 2 (2021): 12-28. https://doi.org/10.37934/cfdl.13.2.1228
[14] Mahat, Rahimah, Muhammad Saqib, Imran Ulah, Sharidan Shafie, and Sharena Mohamad Isa. "MHD Mixed Convection of Viscoelastic Nanofluid Flow due to Constant Heat Flux." *Journal of Advanced Research in Numerical Heat Transfer* 9, no. 1 (2022): 19-25.

[15] Bakar, Fairul Naim Abu, and Siti Khuzaimah Soid. "MHD stagnation-point flow and heat transfer over an exponentially stretching/shrinking vertical sheet in a micropolar fluid with a Buoyancy effect." *Journal of Advanced Research in Numerical Heat Transfer* 8, no. 1 (2022): 50-55.
[16] Ganjikunta, Aruna, Hari Babu Kommaddi, Venkateswarlu Bhajanthri, and Raghunath Kodi. "An unsteady MHD flow of a second-grade fluid passing through a porous medium in the presence of radiation absorption exhibits Hall and ion slip effects." *Heat Transfer* 52, no. 1 (2023): 780-806. https://doi.org/10.1002/htj.22716
[17] Raizah, Zehba AS, Sameh E. Ahmed, Dalal Alrowaili, M. A. Mansour, and Z. Morsy. "Magnetic micropolar nanofluids flow in double lid-driven enclosures using two-energy equation model." *Heat Transfer* 50, no. 3 (2021): 2743-2763. https://doi.org/10.1002/htj.22003
[18] Motsa, Sandile Sydney, and Isaac L. Animasaun. "A new numerical investigation of some thermo-physical properties on unsteady MHD non-Darcian flow past an impulsively started vertical surface." *Thermal Science* 19, no. suppl. 1 (2015): 249-258. https://doi.org/10.2298/TSCI15S1S49M
[19] Sarada, Konduru, Ramanahalli J. Punith Gowda, Ioannis E. Sarris, Rangaswamy Naveen Kumar, and Ballajja C. Prasannakumara. "Effect of magnetohydrodynamics on heat transfer behaviour of a non-Newtonian fluid flow over a stretching sheet under local thermal non-equilibrium condition." *Fluids* 6, no. 8 (2021): 264. https://doi.org/10.3390/fluids6080264
[20] Parhizi, Mohammad, Mohsen Torabi, and Ankur Jain. "Local thermal non-equilibrium (LTNE) model for developed flow in porous media with spatially-varying Biot number." *International Journal of Heat and Mass Transfer* 164 (2021): 120538. https://doi.org/10.1016/j.ijheatmasstransfer.2020.120538
[21] Alsabery, A. I., A. J. Chamkha, I. Hashim, and P. G. Siddheshwar. "Effects of nonuniform heating and wall conduction on natural convection in a square porous cavity using LTNE model." *Journal of Heat Transfer* 139, no. 12 (2017): 122008. https://doi.org/10.1115/1.4037087
[22] Ouyang, Xiao-Long, Pei-Xue Jiang, and Rui-Na Xu. "Thermal boundary conditions of local thermal non-equilibrium model for convection heat transfer in porous media." *International journal of heat and mass transfer* 60 (2013): 31-40. https://doi.org/10.1016/j.ijheatmasstransfer.2012.12.017
[23] Pramanik, S. "Casson fluid flow and heat transfer past an exponentially porous stretching surface in presence of thermal radiation." *Ain shams engineering journal* 5, no. 1 (2014): 205-212. https://doi.org/10.1016/j.asej.2013.05.003
[24] Mohamed, Muhammad Khairul Anuar, Siti Hanani Mat Yasin, and Mohd Zuki Salleh. "Slip Effects on MHD Boundary Layer Flow over a Flat Plate in Casson Ferrofluid." *Journal of Advanced Research in Fluid Mechanics and Thermal Sciences* 88, no. 1 (2021): 49-57. https://doi.org/10.37934/arfmts.88.1.4957
[25] Khan, Kashif Ali, Faizan Jamil, Javaid Ali, Ilyas Khan, Nauman Ahmed, Mulugeta Andualem, and Muhammad Rafiq. "Analytical simulation of heat and mass transmission in casson fluid flow across a stretching surface." *Mathematical Problems in Engineering* 2022 (2022): 1-11. https://doi.org/10.1155/2022/5576194
[26] Mukhopadhyay, Swati, and Kuppalapalle Vajravelu. "Diffusion of chemically reactive species in Casson fluid flow over an unsteady permeable stretching surface." *Journal of Hydrodynamics, Ser. B* 25, no. 4 (2013): 591-598. https://doi.org/10.1016/S1001-6058(11)60400-X
[27] Hamid, M., M. Usman, Z. H. Khan, R. Ahmad, and W. Wang. "Dual solutions and stability analysis of flow and heat transfer of Casson fluid over a stretching sheet." *Physics Letters A* 383, no. 20 (2019): 2400-2408. https://doi.org/10.1016/j.physleta.2019.04.050
[28] Nadeem, Sohail, Rizwan Ul Haq, Noreen Sher Akbar, and Zafar Hayat Khan. "MHD three-dimensional Casson fluid flow past a porous linearly stretching sheet." *Alexandria Engineering Journal* 52, no. 4 (2013): 577-582. https://doi.org/10.1016/j.aej.2013.08.005
[29] Mustafa, Meraj, Tasawar Hayat, Pop Ioan, and Awatif Hendi. "Stagnation-point flow and heat transfer of a Casson fluid towards a stretching sheet." *Zeitschrift für Naturforschung A* 67, no. 1-2 (2012): 70-76. https://doi.org/10.5560/zna.2011-0057
[30] Rehman, Khalil Ur, Aneeqa Ashfaq Malik, M. Y. Malik, N. Sandeep, and Noor Ul Saba. "Numerical study of double stratification in Casson fluid flow in the presence of mixed convection and chemical reaction." *Results in physics* 7 (2017): 2997-3006. https://doi.org/10.1016/j.rinp.2017.08.020
[31] Hayat, T., S. A. Shehzad, and A. Alsaedi. "Soret and Dufour effects on magnetohydrodynamic (MHD) flow of Casson fluid." *Applied Mathematics and Mechanics* 33 (2012): 1301-1312. https://doi.org/10.1007/s10483-012-1623-6
[32] Ramzan, Muhammad, Anwar Saeed, Poom Kumam, Zubair Ahmad, Muhammad S. Junaid, and Dolat Khan. "Influences of Soret and Dufour numbers on mixed convective and chemically reactive Casson fluids flow towards an inclined flat plate." *Heat Transfer* 51, no. 5 (2022): 4393-4433. https://doi.org/10.1002/htj.22505
[33] Kumar, M. Anil, Yanala Dharmendar Reddy, B. Shankar Goud, and V. Srinivasa Rao. "An impact on non-Newtonian free convective MHD Casson fluid flow past a vertical porous plate in the existence of Soret, Dufour, and chemical

reaction." *International Journal of Ambient Energy* 43, no. 1 (2022): 7410-7418. https://doi.org/10.1080/01430750.2022.2063381

[34] Puneeth, Venkatesh, Sarpabhushana Manjunatha, Bijjanal Jayanna Gireesha, and Rama Subba Reddy Gorla. "Magneto convective flow of Casson nanofluid due to Stefan blowing in the presence of bio-active mixers." *Proceedings of the Institution of Mechanical Engineers, Part N: Journal of Nanomaterials, Nanoengineering and Nanosystems* 235, no. 3-4 (2021): 83-95. https://doi.org/10.1177/23977914211016692

[35] Uddin, Mohammed Jashim, Yasser Alginahi, O. Anwar Bég, and Muhammad Nomani Kabir. "Numerical solutions for gyrotactic bioconvection in nanofluid-saturated porous media with Stefan blowing and multiple slip effects." *Computers & Mathematics with Applications* 72, no. 10 (2016): 2562-2581. https://doi.org/10.1016/j.camwa.2016.09.018

[36] Tuz Zohra, Fatema, Mohammed Jashim Uddin, Md Faisal Basir, and Ahmad Izani Md Ismail. "Magnetohydrodynamic bio-nano-convective slip flow with Stefan blowing effects over a rotating disc." *Proceedings of the Institution of Mechanical Engineers, Part N: Journal of Nanomaterials, Nanoengineering and Nanosystems* 234, no. 3-4 (2020) : 83-97. https://doi.org/10.1177/2397791419881580

[37] Latiff, N. A., M. J. Uddin, and AI Md Ismail. "Stefan blowing effect on bioconvective flow of nanofluid over a solid rotating stretchable disk." *Propulsion and power research* 5, no. 4 (2016): 267-278. https://doi.org/10.1016/j.jppr.2016.11.002

[38] Yusof, Nur Syamila, Siti Khuzaimah Soid, Mohd Rijal Illias, Ahmad Sukri Abd Aziz, and Nor Ain Azeany Mohd Nasir. "Radiative Boundary Layer Flow of Casson Fluid Over an Exponentially Permeable Slippery Riga Plate with Viscous Dissipation." *Journal of Advanced Research in Applied Sciences and Engineering Technology* 21, no. 1 (2020): 41-51. https://doi.org/10.37934/araset.21.1.4151

[39] Fang, Tiegang, and Wei Jing. "Flow, heat, and species transfer over a stretching plate considering coupled Stefan blowing effects from species transfer." *Communications in Nonlinear Science and Numerical Simulation* 19, no. 9 (2014): 3086-3097. https://doi.org/10.1016/j.cnsns.2014.02.009